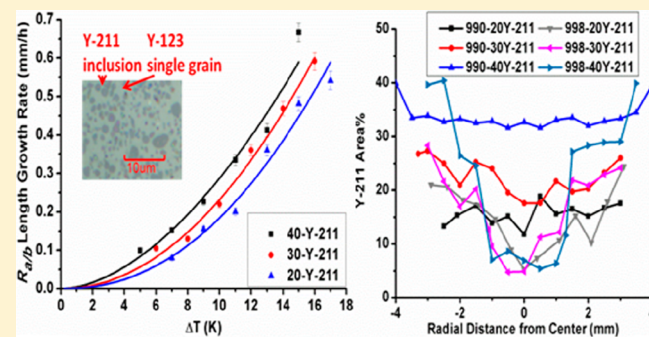


# The Influence of Y-211 Content on the Growth Rate and Y-211 Distribution in Y–Ba–Cu–O Single Grains Fabricated by Top Seeded Melt Growth

Wei Zhai,\* Yunhua Shi, John H. Durrell, Anthony R. Dennis, and David A. Cardwell

Department of Engineering, University of Cambridge, Trumpington Street, Cambridge CB2 1PZ, U.K.

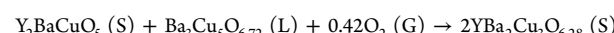
**ABSTRACT:** The melt processing of Y–Ba–Cu–O (YBCO) single grains has been investigated using different isothermal temperature profiles for precursor powders containing varying amounts of Y-211. The crystal morphology of the as-grown YBCO single grains and the growth rate, which is influenced critically by the initial Y-211 content and the under-cooling temperature, have been analyzed. A simple method to determine an optimum temperature profile for the growth of bulk YBCO single grains has been proposed based on the results of this investigation. The influence of the initial Y-211 content on the macrosegregation of Y-211 inclusions for the different crystallographic orientations and different under-cooling temperatures has been analyzed. The correlation between the initial Y-211 content and the macrosegregation of Y-211 inclusions within the YBCO single grain along the different growth directions is interpreted from the growth rate data using Y-diffusion mechanism and pushing/trapping theory. Finally, an improved method for fabricating bulk YBCO superconductors containing a uniform distribution of pinning centers in the single grain, which has significant potential for improving the superconducting properties of bulk YBCO superconductors for practical applications, is proposed.



## 1. INTRODUCTION

Bulk Y–Ba–Cu–O (YBCO) superconductors have significant potential for high field, permanent magnet applications<sup>1</sup> such as flywheel energy storage systems<sup>2</sup> and magnetic bearings<sup>3</sup> because of their ability to trap large magnetic fields at the boiling point of liquid nitrogen (77 K).<sup>4</sup> The top-seeded melt-growth (TSMG) technique<sup>5</sup> is accepted widely as an effective way to grow bulk, single grain YBCO superconductors that exhibit homogeneous single grain structure<sup>6</sup> with high critical current density ( $J_c$ )<sup>7</sup> and associated high field trapping potential<sup>4</sup> for practical applications.<sup>8</sup> However, it is essential to develop a reliable TSMG fabrication process because of the relatively high price of the raw materials and the long fabrication times (typically 7 days for a YBCO sample of 25 mm diameter) of single grains if this method is to be used for the large scale fabrication and application of these technologically important materials.

An optimum temperature profile is accepted widely to be crucial to the successful growth of bulk YBCO single grains.<sup>9</sup> In the TSMG technique,  $\text{YBa}_2\text{Cu}_3\text{O}_{7-\delta}$  (Y-123) decomposes peritectically at the melting temperature ( $T_m$ ) to form a solid  $\text{Y}_2\text{BaCuO}_5$  (Y-211) phase and yttrium-deficient Ba–Cu–O liquid phase.<sup>5</sup> The Y-123 single grain nucleates epitaxially from a seed, which has a higher melting temperature and a similar crystal structure to the Y-123 phase, as the temperature is decreased below the peritectic solidification temperature ( $T_s$ ) on cooling, as described by the following reaction:<sup>5</sup>



where S, L, and G indicate solid, liquid, and gas phases, respectively. The probability for the random nucleation of satellite YBCO grains increases to a critical level as the temperature decreases further to the self-nucleation temperature ( $T_r$ ), which effectively marks the end of the growth window. Therefore, the TSMG process is sensitive to both  $T_s$  and  $T_r$ , which must be optimized if various undesirable effects, such as incomplete melting and the formation of satellite YBCO grains, are to be avoided.<sup>10</sup> The optimum values of  $T_s$ ,  $T_r$ , and growth rate are different if the precursor powders contain different compositions. In addition, every furnace has unique thermal features, so a simple method of determining the optimum temperature profile for a given precursor powder composition is important if bulk YBCO superconductors are to be grown successfully and reliably for commercial applications.<sup>9,10</sup>

A homogeneous distribution of Y-211 inclusions in the as-grown Y-123 matrix is considered to be a particularly important aim of the growth process for the manufacture of large, YBCO superconducting grains that exhibit a uniform, high  $J_c$  value.<sup>11,12</sup> The homogeneity of the Y-211 particle distribution is also fundamental to achieve good mechanical properties in fully

Received: July 28, 2014

Revised: September 18, 2014

Published: October 29, 2014

processed single grains.<sup>13,14</sup> Additional Y-211 particles are generally added to the precursor powders in the TSMG process to reduce the liquid phase loss and to act as a supporting skeleton during the melting process.<sup>15,16</sup> The supply of yttrium ions for the peritectic solidification reaction, which are generated by Y-211 particles that dissolve in the Ba–Cu–O liquid at the growth front, is determined principally by the Y-diffusion theory.<sup>17</sup> Unreacted, undissolved small Y-211 particles are typically trapped in the as-grown Y-123 single grain as a consequence, which creates Y-211/Y-123 interfaces that are considered generally to form effective flux pinning centers and to improve the  $J_c$  value of the single grains.<sup>18</sup> In particular, the  $J_c$  value is reported to increase with the  $V_{211}/d_{211}$  ratio, where  $V_{211}$  is the Y-211 volume fraction, and  $d_{211}$  is the average size of the Y-211 particles.<sup>19,20</sup> The size of Y-211 particles may be refined generally by adding coarsening inhibitor additives to the precursor powders, such as Pt<sup>21</sup> and CeO<sub>2</sub>.<sup>22</sup> The distribution of Y-211 inclusions, however, has been reported to be sensitive to the crystallographic orientation and the growth rate of the Y-123 grain.<sup>23–26</sup> It has been reported specifically that the number density of Y-211 particles increases continuously with distance from the position of the seed toward the edge of the large grain sample in YBCO superconductors containing Pt.<sup>23</sup> The number and size distribution of trapped Y-211 particles within the Y-123 matrix are typically smaller along the *c*-axis growth direction than that along the *a/b*-axis.<sup>24,25</sup>

A graded-TSMG fabrication technique has been developed previously to grow bulk YBCO superconductors containing a uniform distribution of Y-211 inclusions.<sup>26</sup> This involved the preparation of three types of precursor powders with different concentrations of Y-211, arranged separately in a U-shape geometry through the cross-section of a cylindrical green body, with the precursor powder containing 40 wt % of Y-211 at the center, and those containing 30 wt % and 20 wt % in the middle and in the outer U-layers of the sample, respectively.<sup>26</sup> The graded samples tend to exhibit a uniform distribution of Y-211 inclusions along the direction parallel to the crystallographic *c*-axis after the graded-TSMG process. However, the distribution of Y-211 inclusions along the *a/b*-axis of the samples is highly nonuniform.<sup>26</sup> To improve the graded-TSMG technique further, it is necessary to understand the influence of the initial Y-211 content on the macrosegregation of Y-211 inclusions under different crystallographic orientation as well as under conditions of different under-cooling.

The mechanism of the observed macrosegregation of Y-211 particles in melt-processed YBCO has not been clarified completely to date, although the particle pushing/trapping theory<sup>27</sup> has been used to some extent to explain this phenomenon.<sup>23–26</sup> According to this theory, Y-211 particles of size larger than a critical radius will be trapped within the growing YBCO single grain,<sup>23</sup> with the critical radius being inversely proportional to the growth rate.<sup>23</sup> Therefore, the influence of the initial Y-211 content on the growth rate requires further investigation to understand the macrosegregation phenomenon of Y-211 inclusions. Xu et al. proposed from crystal morphology studies that the growth rate of Y-123 containing higher amounts of Y-211 is greater than that for a lower Y-211 content.<sup>28,29</sup> However, the relation between the Y-211 content and growth rate has not yet been analyzed systematically or quantitatively.

In this paper, the influence of initial Y-211 content on the growth rate is analyzed systematically for different crystallographic orientations and under-cooling temperature. Three

types of precursor powders containing different weight percentages of Y-211 (40 wt %, 30 wt %, and 20 wt %) were prepared for this investigation. YBCO single grains were prepared in batches from the three types of precursor powders using different isothermal temperature profiles, and the crystal morphology of the as-grown YBCO single grains were analyzed. The growth rate of YBCO single grains, which was influenced significantly by the initial Y-211 content and the under-cooling temperature, has been analyzed systematically. A simple method of determining an optimum temperature profile for the growth of bulk YBCO single grains is proposed based on the results of this study.

Finally, the influence of the initial Y-211 content on the macrosegregation of Y-211 inclusions for different crystallographic orientations and under-cooling temperatures have been analyzed and discussed based on the growth rate data. The Y-diffusion mechanism and particle pushing/trapping theory have been used to explain the observed phenomenon. An improved method for the fabrication of bulk YBCO superconductors containing a uniform distribution of pinning centers within the single grain matrix, which has significant potential for improving the superconducting properties of bulk YBCO superconductors for practical applications, has consequently been proposed.

## 2. EXPERIMENTAL PROCEDURE

**2.1. Preparation of Precursor Powders.** Precursor powders were prepared by mixing thoroughly commercially available Y-123, Y-211 (purity of 99.9%, supplied by the Toshima Manufacturing Co. Ltd.), and CeO<sub>2</sub> (purity of 99.9%, supplied by Alfa Aesar) in different weight ratios using a motorized pestle and mortar. The particle sizes of the Y-123 and Y-211 powders were 2–3  $\mu\text{m}$  and approximately 1  $\mu\text{m}$ , respectively. In total, three types of precursor powders were prepared as part of this study: (i) 40-Y-211, in a composition ratio of Y-123:Y-211:CeO<sub>2</sub>, a ratio of 60:40:1 by weight; (ii) 30-Y-211, in a composition ratio of 70:30:1; and (iii) 20-Y-211 in a composition ratio of 80:20:1. N-40-Y-211 precursor powder was also prepared with the same weight ratio as 40-Y-211, but the Y-211 powders were supplied by Nexans, which had an average particle size of approximately 9  $\mu\text{m}$  (i.e., significantly larger than the Y-211 powders supplied by the Toshima Manufacturing Co. Ltd.).

**2.2. Fabrication of YBCO Samples by Isothermal Under-Cooling.** Green bodies of the 40-Y-211, 30-Y-211, and 20-Y-211 pellets were made by pressing the precursor powders uniaxially into cylindrical pellets of approximate diameter 16.0 mm and thickness 8.0 mm under loads of between 2 and 3 tons. An NdBCO single crystal seed, cleaved along the *a/b* plane, was placed at the center of the upper surface of each green pellet prior to batch melt processing using isothermal TSMG in the same box furnace. The isothermal temperature profile used in this study is shown in Figure 1. The green pellets were heated initially to 1065 °C, held for 1 h to decompose fully the Y-123 phase into Y-211 and the Ba–Cu–O liquid phase, and cooled at a rate of 75 °C/h to the growth temperature ( $T_g$ ).

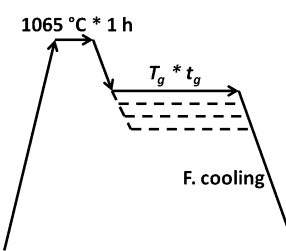


**Figure 1.** Isothermal temperature profile used to fabricate YBCO single grains.

The samples were then grown at the isothermal  $T_g$  for a fixed growth time ( $t_g$ ) and were then furnace cooled quickly to room temperature. It was assumed that the growth morphology was unaffected during rapid cooling following the isothermal growth process. The growth temperature and time was varied from 1012–986 °C in intervals of 2 °C and from 40–2 h, respectively.

**2.3. Fabrication of Bulk YBCO Samples by Continuous Cooling.** The TSMG technique using a continuous under-cooling temperature profile has been used to grow graded YBCO single grains as reported previously.<sup>26</sup> The graded samples had three types of precursor powders arranged in a U-shape geometry through the cross-section of the cylindrical green body, with the 40-Y-211 precursor powders at the center and the 30-Y-211 and 20-Y-211 powders in the middle and outer layers of the pellet, respectively (as shown in Figure 2). An N-graded sample, containing the N-40-Y-211 precursor

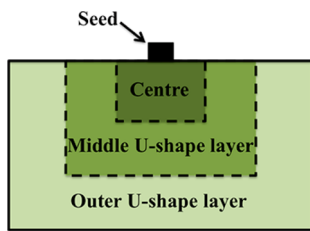


Figure 2. Schematic diagram of the cross-section view of the graded sample.

powders at the center of the pellet, and a P-graded sample, containing purely Y-211 powders (Toshima Manufacturing Co. Ltd.) at the center, were prepared as part of the present study. The middle and outer layers of the N-graded and P-graded samples contained the same precursor powder composition as the graded samples reported in the earlier study.

**2.4. DTA Analysis.** The melting point of the precursor powders was measured by differential thermal analysis (DTA). DTA was performed continuously from room temperature to 1200 °C at a rate of 5 °C/min under a flowing air environment at a rate of 5 cm<sup>3</sup>/min. The data were collected using a LabSys Evo DTA Instrument.

**2.5. Growth Rate Measurement.** The size of the YBCO single grains grown using the isothermal temperature profiles was determined critically by  $T_g$  and  $t_g$ . The growth rate ( $R$ ) was calculated from the ratio of the growth length parallel to the growth direction to the growth time, with the growth length parallel to the  $a/b$ -axis ( $L_{a/b}$ ), which is defined as the distance from the edge of the seed to the solid–liquid interface,<sup>30</sup> as illustrated schematically in Figure 3, panel

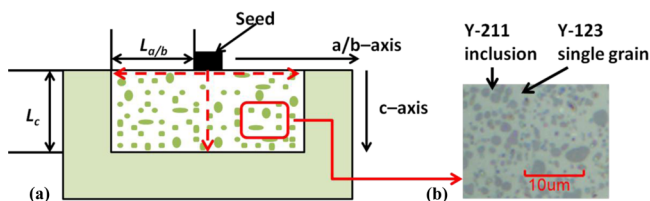


Figure 3. (a) Schematic cross-section of a single grain. (b) Optical micrograph that shows that the Y-211 inclusions are embedded in the Y-123 single grain matrix.

a. The growth length parallel to the  $c$ -axis ( $L_c$ ) was defined as the length from the top surface of the sample to the solid–liquid interface<sup>30</sup> (also shown schematically in Figure 3a). This enables the  $R$  value for different  $T_g$  values to be calculated via the following equations:

$$\text{Length growth rate: } R_{a/b} = L_{a/b}/t_g$$

$$\text{Height growth rate: } R_c = L_c/t_g$$

**2.6. Measurement of the Y-211 Distribution.** Samples grown from 40-Y-211, 30-Y-211, and 20-Y-211 precursor powders using an isothermal temperature profile were cut in half through the seed using a diamond wheel. The exposed cross-sections were ground successively using 500, 800, 1000, 1200, and 2400 grit SiC paper and polished additionally with 3, 1, and 0.25  $\mu\text{m}$  diamond spray using only ethanol for lubrication during the polishing process. Optical images at a magnification of 1000 times were taken along both the  $a/b$ -axis and  $c$ -axis of the YBCO samples at intervals of 0.5 mm using a Moticam Pro 282A optical microscope. As the dashed lines indicated in Figure 3 panel a, the observation was made beneath the top surface along the  $a/b$ -axis and from the center of the seed along the  $c$ -axis. The optical micrographs were analyzed using ImageJ software to determine the area fraction of the Y-211 inclusions embedded in the Y-123 grains, as illustrated by the optical micrograph in Figure 3, panel b.

The top surfaces of the N-graded and P-graded samples were polished using the procedure described above. Optical images were taken at regular positions from the seed to the edge of the sample and analyzed to investigate the Y-211 distribution along the  $a/b$ -axis across the top surfaces of the samples.

### 3. RESULTS AND DISCUSSION

**3.1. Influence of Initial Y-211 Content on the Peritectic Solidification Temperature.** Figure 4, panel (a) shows the DTA traces of precursor powders 40-Y-211, 30-Y-211, and 20-Y-211, from which it can be seen that the peak position of the temperature curves of these powders are approximately 1014 °C, 1017 °C, and 1019 °C, respectively. The shift of the peak position of the temperature curves represents that the kinetic of the peritectic decomposition temperature of the precursor powders decreases as the Y-211 content increases, as indicated by the dashed line in Figure 4, panel a. Shi et al.<sup>30</sup> reported previously that the trend in the kinetic of peritectic melting temperature is indicative of the trend in the peritectic solidification temperature of the precursor powders. Therefore, initial peritectic solidification in the vicinity of the seed crystal may take place earlier in the thermal process (i.e., at higher temperature) for the green precursor bodies with a low concentration of Y-211 inclusions compared to those with a higher Y-211 inclusion density.

A batch of samples of each composition were prepared at a different isothermal temperature  $T_g$  within a range between 1012 and 986 °C for different  $t_g$  values, as shown in Table 1.  $T_g$  was chosen initially to be 1012 °C to determine the  $T_s$  value for the different precursor powders, which is slightly lower than the peak position of the DTA temperature curves of the three precursor powders investigated. No single grain growth from the seed crystal was observed above 1007 °C, at which growth for 30 h results in the appearance of a small, bright, black Y-123 single grain in the vicinity of the seed crystal in the 20-Y-211 sample (Figure 4b). No Y-123 single grain growth was observed at 1007 °C for samples 30-Y-211 and 40-Y-211. Isothermal growth at 1006 °C for 30 h, however, yielded Y-123 single grain growth at the position of the seed crystal in both the 20-Y-211 and 30-Y-211 samples, although no growth was observed in the 40-Y-211 sample at this temperature. Similarly, it was assumed from the results that the values of  $T_s$  for samples 40-Y-211, 30-Y-211, and 20-Y-211 precursor pellets were 1005 °C, 1006 °C, and 1007 °C, respectively. It can be concluded from analysis of the surface morphologies that the peritectic solidification temperature is higher for the precursor pellets containing lower amounts of Y-211, which is in good agreement with the results of the DTA analysis.

**3.2. Growth Rate Analysis.** Table 1 shows photographs of the batch-processed YBCO single grains fabricated using the

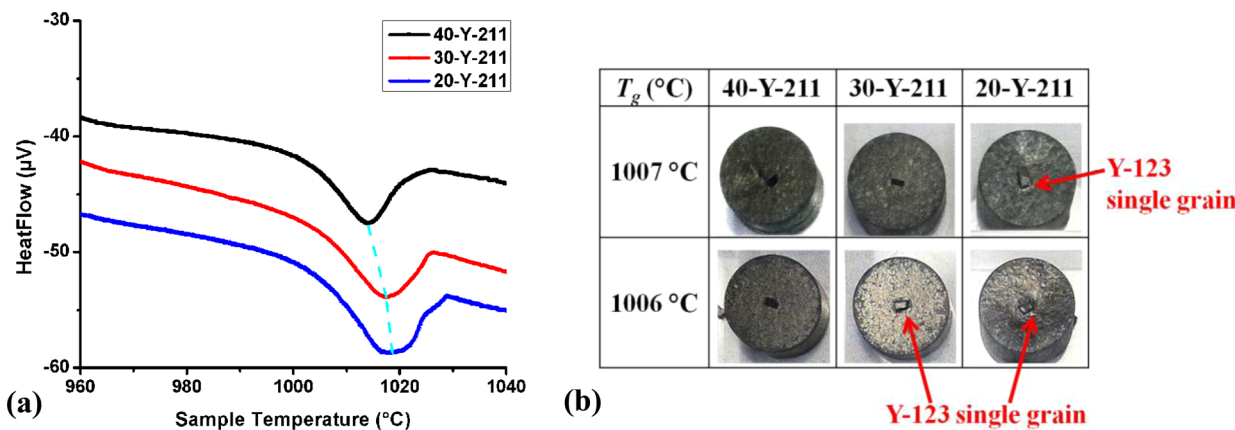


**Figure 4.** (a) DTA traces for the 40-Y-211, 30-Y-211, and 20-Y-211 precursor powders. (b) Photographs of the top surface of the samples grown isothermally at 1007 and 1006 °C.

**Table 1. Photographs of YBCO Single Grains Fabricated Using the Isothermal Under-Cooling Method**

$T_g$ (°C)	$t_g$ (h)	40-Y-211	30-Y-211	20-Y-211
1000	20			
998	20			
996	15			
994	10			
992	8			
990	6			
988	4			
986	2			

isothermal under-cooling method. The growth temperature was varied from 1012–986 °C at intervals of 2 °C, with growth times that varied between 40 and 2 h. The growth rate of these samples, which was influenced critically by the initial Y-211 content and the under-cooling temperature, was analyzed systematically, as described below.

**3.2.1. Influence of Under-Cooling Temperature on Growth Rate.** The growth rate for all of the compositions studied along both the  $a/b$ -axis ( $R_{a/b}$ ) and  $c$ -axis ( $R_c$ ) as a function of under-cooling temperature ( $\Delta T = T_s - T_g$ ) is shown in Figure 5. It is significant that the  $R$  value measured in both directions and increased with increased  $\Delta T$  in each case. This is because the under-cooling temperature contributes to the main driving force for interface kinetics and diffusion of solute.<sup>31,32</sup> As a result, the rate of the peritectic solidification reaction increases as the under-cooling increases along both growth directions for all of the precursor compositions investigated. Endo et al.<sup>32</sup> proposed that the relation between the growth rate and under-cooling follows the power law equation,  $R = \alpha(\Delta T)^\beta$  (where  $\alpha$  and  $\beta$  are constants). The parameter fits to this power law for each composition for both growth directions are shown in Table 2, from which it can be seen that  $\alpha$  and  $\beta$  change systematically for the different compositions and growth directions.

**3.2.2. Influence of Initial Y-211 Content on the Growth Rate.** It can be seen from Figure 5 that the growth rate in both crystallographic directions increases with the increase of the initial Y-211 content in the precursor powders. This is because the necessary  $\text{Y}^{3+}$  solute required for growth of the Y-123 phase is supplied by diffusion from Y-211 inclusions dispersed in the Ba–Cu–O liquid through the liquid phase.<sup>13</sup> The  $\text{Y}^{3+}$  diffusion rate is, therefore, considered the rate-limiting factor for the growth of Y-123 single grains.<sup>13</sup> The overall amount of Y-211 inclusions in the precursor powders increases in ascending order for the 20-Y-211, 30-Y-211, and 40-Y-211 samples. Therefore, the excess of Y-211 content in the precursor powders increases the amount of Y-211 inclusions for the supply of  $\text{Y}^{3+}$  for the growth of the Y-123 single grain, which contributes to a higher  $R$  value. It is, however, noticeable that the difference in growth rate between each composition is not very large under conditions of lower under-cooling temperature (i.e., below 6 °C). This is because the growth rate is very small at lower under-cooling, which leaves sufficient time for the  $\text{Y}^{3+}$  ions to diffuse from the Y-211 inclusion sources. The main rate-limiting factor in this case is the low driving force due to the

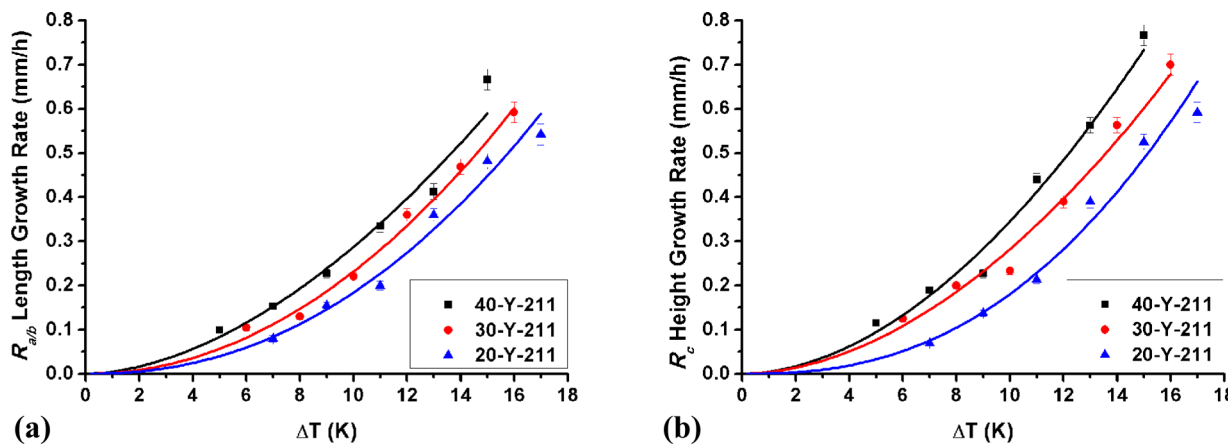


**Figure 5.** Growth rate measured (a) across the sample diameter ( $R_{a/b}$ ) and (b) through the sample thickness ( $R_c$ ) as a function of under-cooling temperature for the 40-Y-211, 30-Y-211, and 20-Y-211 samples.

**Table 2. Growth Rate Parameters for the 40-Y-211, 30-Y-211, and 20-Y-211 Samples**

sample		$\alpha$	$\beta$
40-Y-211	$R_{a/b}$	0.00486	1.77238
	$R_c$	0.00475	1.86164
30-Y-211	$R_{a/b}$	0.00218	2.02725
	$R_c$	0.00386	1.86399
20-Y-211	$R_{a/b}$	0.00119	2.19071
	$R_c$	0.00065	2.4449

very low under-cooling temperature, so the influence of initial Y-211 content on growth rate is not significant. As the undercooling temperature increases, the growth rate increases accordingly, and the precursor powders containing a higher concentration of Y-211 are able to supply  $Y^{3+}$  faster. Hence, the difference in growth rate for the different composition becomes large.

**3.3. Growth of Bulk YBCO Single Grains by Adjusting the Temperature Profile.** The growth morphology of samples grown at different isothermal  $T_g$  and  $t_g$  can be compared and analyzed from Table 1. Three important temperature points for an optimum temperature profile,  $T_s$ ,  $T_r$  and the superior growth temperature range, can be determined by analyzing the growth morphology and growth rate of samples grown at different isothermal  $T_g$ . Figure 6 shows the simplified temperature profiles and photographs of the top

surface of the YBCO single grains of diameter of  $\sim 25$  mm and  $\sim 32$  mm, respectively.

The growth window for a given temperature profile usually starts at a temperature just above  $T_s$  for a complete peritectic solidification reaction and ends at a temperature around  $T_r$  to prevent unwanted random nucleation of satellite YBCO grains. Therefore,  $T_s$  and  $T_r$  determine the growth window of the temperature profile. As discussed in section 3.1, the values of  $T_s$  for the 40-Y-211, 30-Y-211, and 20-Y-211 precursor powders are 1005 °C, 1006 °C and 1007 °C, respectively. Randomly nucleated satellite YBCO grains start to form in the 20-Y-211 sample at the edge of the as-grown YBCO single grain at 990 °C, while the other two samples exhibit a clear, square-shaped YBCO single grain, as can be seen in Table 1. Therefore, the  $T_r$  value for the 20-Y-211 sample is  $\sim 990$  °C. Similarly, the  $T_r$  values for the 30-Y-211 and 40-Y-211 samples can be determined as  $\sim 988$  °C and  $\sim 986$  °C, respectively. This indicates clearly that  $T_r$  for the precursor powders decreases as the Y-211 content increases. The temperature window for the bulk YBCO single grain grown from the 40-Y-211, 30-Y-211, and 20-Y-211 precursor powders can be calculated accordingly. The growth window was consequently reduced from 1008–987 °C for a cooling rate of 0.3 °C/h to grow a YBCO single grain of  $\sim 25$  mm diameter based on the results of this analysis, as shown in Figure 6, panel a. The photograph of the sample in Figure 6, panel (a) shows the fully grown YBCO single grain fabricated by this process.

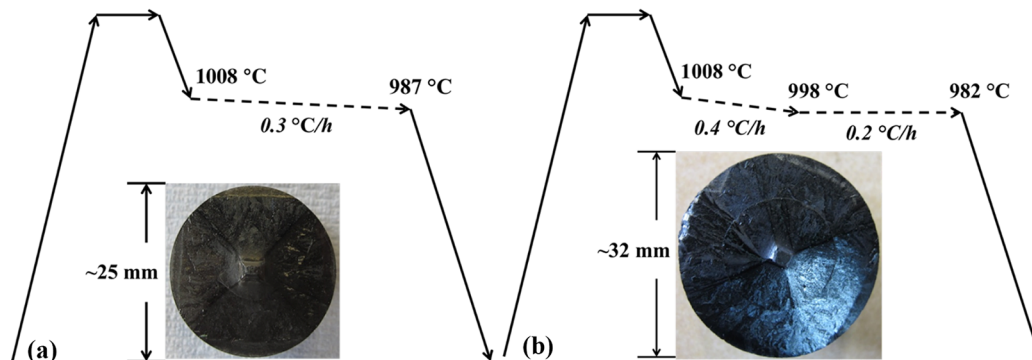


**Figure 6.** Temperature profiles and photographs of the top surface for the growth of bulk YBCO single grains with diameters of (a)  $\sim 25$  mm and (b)  $\sim 32$  mm.

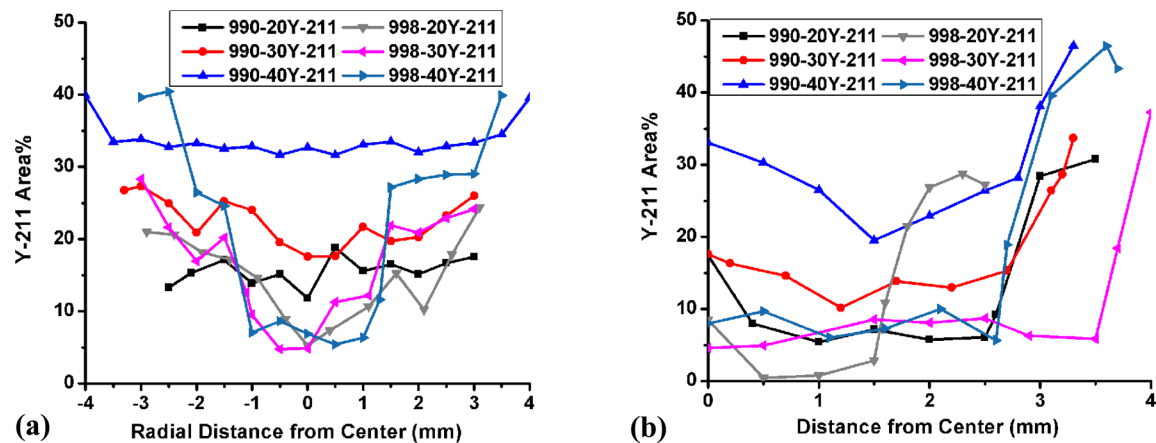


**Figure 7.** Distribution of the area fraction of Y-211 inclusions as a function of distance from the seed crystal along (a) the *a/b*-axis growth direction and (b) the *c*-axis growth direction.

There are two methods for growing YBCO single grains with a diameter larger than 25 mm. The first involves an increase in the range of the growth window. As discussed above, the  $T_r$  value of the precursor powders decreases as the Y-211 content increases. It will be discussed later that the Y-211 content increases as the Y-123 growth front progresses. As a result, the end temperature of the growth window can be reduced to increase the growth time, as shown in Figure 6, panel b (the growth window end temperature has been reduced from 987–982 °C). However, the growth window is limited further by the physical and chemical properties of the precursor powders. Second, the rate of decrease in temperature during peritectic solidification can be reduced to achieve a longer growth time. It can be seen from Table 1 that the samples grown from all three precursor compositions show a clear, square YBCO single grain shape within an isothermal processing temperature range of between 998 and 992 °C. The growth morphology indicates that these YBCO single grains are of good quality. The growth rates for these samples lie in the range of 0.1–0.6 mm/h for a temperature range between 998 and 992 °C, for which the YBCO single grains exhibit both good crystal quality and large growth rate. To grow larger YBCO single grains, the slow cool rate in this critical temperature range can be reduced further, which we define subsequently as the superior growth temperature range.

The growth window was divided subsequently into two parts, as shown in Figure 6, panel b. In the first part (1008–998 °C), the cooling rate is maintained at 0.4 °C/h, since the growth rate in this temperature range is very low. In the second part (998–982 °C), the cooling rate is reduced to 0.2 °C/h, since the growth rate in this temperature is relatively large, and the quality of crystal growth in this range is good. A photograph of a single grain YBCO sample of diameter of ~32 mm grown successfully by this process is shown in Figure 6, panel b.

It can be concluded from this analysis that the growth and characterization of small YBCO samples using an isothermal temperature profile is a relatively simple method for determining an optimum temperature profile for a given precursor composition. Significantly, this method may be applied to the growth of all bulk single grains within the more general (RE)BCO family (where RE = Y, Gd, Sm, Nd, etc.).

**3.4. Influence of Under-Cooling Temperature on the Y-211 Inclusion Distribution.** Y-211 distribution analysis was performed on the YBCO single grains grown at 998 and

990 °C. The area fraction of the Y-211 inclusions within each optical micrograph was plotted as a function of distance from the seed crystal to investigate the Y-211 inclusion distribution along the *a/b*-axis (Figure 7a) and *c*-axis growth directions (Figure 7b), respectively.

It can be seen from the 990–40-Y-211 bright blue curve in Figure 7, panel (a) that the *Area%* of the Y-211 inclusions in the 990–40-Y-211 sample is around 33% along the *a/b* axis. As the growth temperature increases to 998 °C, the *Area%* of the Y-211 inclusions is below 10% within a distance of approximately 1 mm from the seed, but increases dramatically to approximately 28% over a distance of 1–3 mm, as can be seen from the data for sample 998–40-Y-211. The *Area%* of Y-211 inclusions of the 40-Y-211 sample, therefore, increases as the growth temperature reduces from 998–990 °C along the *a/b*-growth direction. A similar trend is observed for the 40-Y-211 data measured along the *c*-axis, in that the *Area%* of the Y-211 inclusions is higher in the sample grown at 990 °C compared to that grown at 998 °C (Figure 7b). The variation of *Area%* with isothermal processing temperature is similar along both the *a/b*- and *c*-growth directions for the 30-Y-211 and 20-Y-211 samples grown at both 990 and 998 °C, as shown in Figure 7. Therefore, it can be concluded that the *Area%* of Y-211 inclusions within the sample measured along both growth directions increases generally with reduced  $T_g$ , in other words, increased under-cooling temperature.

**3.5. Influence of the Initial Y-211 Content on the Distribution of Y-211 Inclusions.** It can be seen from Figure 7, panels a and b that the variation of Y-211 *Area%* with sample position differs significantly at 998 and 990 °C and that the distribution of Y-211 inclusions at different growth temperatures is influenced by the initial Y-211 content.

The Y-211 spatial distribution curves fluctuate along both the *a/b*- and *c*-growth directions at 990 °C, which represents larger under-cooling temperature. It is clear that the *Area%* of the Y-211 inclusions in the 40-Y-211 samples is higher than in the 30-Y-211 and the 20-Y-211 samples along almost the entire *a/b*- and *c*-growth directions. Only at a distance of around 3 mm away from the seed along the *c*-axis (Figure 7b) is the *Area%* of the Y-211 inclusions in the 20-Y-211 sample slightly higher than in the 30-Y-211 sample. This is because the 20-Y-211 sample reaches the extent of its growth at this position, where the liquid phase containing a large amount of Y-211 inclusions is trapped. Therefore, it can be concluded that the *Area%* of the

Y-211 inclusions for an isothermal growth temperature of 990 °C (i.e., for a larger under-cooling temperature) increases with increasing initial Y-211 content in both growth directions. The *Area%* of Y-211 inclusions at 998 °C, which represents a lower under-cooling temperature, is relatively small in the vicinity of the seed along the *a/b*-growth direction but increases dramatically at a distance of around 1 mm from the seed for all of the composition curves. As a result, there is a region of low Y-211 inclusion density along the *a/b*-growth direction when the samples grow under conditions of lower under-cooling temperature. The difference in *Area%* of Y-211 for the three samples fluctuates within the low Y-211 inclusions region along the *a/b* growth direction. Beyond the low-Y-211 regions, it is clear that the 40-Y-211 sample contains the largest number of Y-211 inclusions, followed by samples 30-Y-211 and 20-Y-211 in descending order. It can also be seen from Figure 7, panel b, which shows the Y-211 distribution along the *c*-growth direction at a growth temperature of 998 °C, that there is also an area where the difference in *Area%* of Y-211 inclusions fluctuates for this growth direction, after which the difference becomes well-defined. In conclusion, at lower under-cooling temperature, a low-Y-211 region exists close to the position of the seed in all YBCO samples studied. The difference in Y-211 inclusion content in the low-Y-211 region fluctuates for the 40-Y-211, 30-Y-211, and 20-Y-211 samples. The Y-211 inclusion content increases as the initial Y-211 content increases for distances from the seed greater than that of the low-Y-211 region.

**3.6. Low-Y-211 Inclusions Area in N-Graded and P-Graded Samples.** The distribution of Y-211 inclusions along the *a/b*-axis on the top surfaces of the N-graded and P-graded samples is shown in Figure 8. The center of the precursor pellet

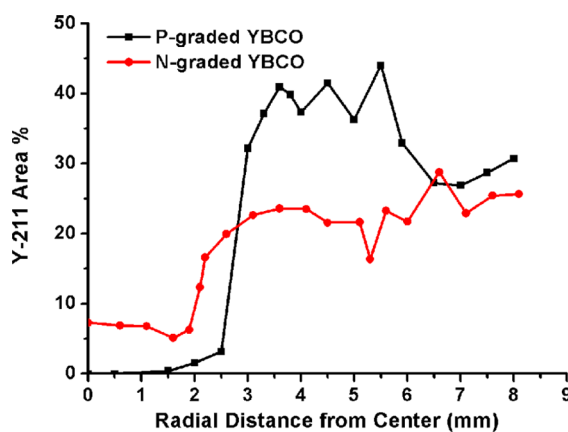


Figure 8. Y-211 distribution along the *a/b*-axis of the top surfaces of the N-graded and P-graded YBCO single grain samples.

contains purely Y-211 powders in the P-graded sample. In the N-graded sample, however, the center of the precursor pellet contains N-40-Y-211 powder, which contains larger sized and a higher concentration of Y-211 particles than the other parts of the sample. However, it can be seen that the Y-211 inclusions exhibit their lowest concentration at the center of both the N-graded and P-graded samples, as shown in Figure 8. As reported previously for the graded YBCO samples,<sup>26</sup> which contain 40-Y-211 powders at their center, 30-Y-211 powders in the middle layer, and 20-Y-211 powders in the outer layer, there is also a region of low-Y-211 immediately below the position of the seed. Standard YBCO samples, which contain

30-Y-211 powders, also exhibit a region of low Y-211 concentration below the seed.<sup>26</sup> Therefore, it may be concluded that such a region exists for all single grain bulk YBCO samples regardless of the presence of an increased concentration of Y-211 powders or Y-211 powders of a larger size at the center of the sample.

**3.7. Analysis of the Y-211 Inclusions Distribution.** The inhomogeneous distribution of Y-211 particles in the YBCO matrix has been studied systematically by Endo et al.,<sup>24,25</sup> who concluded that the macrosegregation of Y-211 depends critically on the growth direction and the growth rate as a function of under-cooling. Endo et al.<sup>24,25</sup> employed a particle pushing/trapping theory to explain this phenomenon by considering “inactive particles” (Y-211) at an advancing solid/liquid interface (i.e., the growth front of the Y-123 phase) during peritectic solidification. The driving force that operates on the particles consists of the drag force due to viscous flow around the particle and the force due to the interfacial energy,  $\Delta\sigma_0$ , which is defined as

$$\Delta\sigma_0 = \Delta\sigma_{sp} - \Delta\sigma_{lp} - \Delta\sigma_{sl}$$

where  $\Delta\sigma_{sp}$ ,  $\Delta\sigma_{lp}$ , and  $\Delta\sigma_{sl}$  are the solid/particle, liquid/particle, and solid/liquid surface energies, respectively. Assuming the Y-211 particle is spherical and that the shape of the interface is planar, the critical radius ( $r^*$ ) depends on the growth rate ( $R$ ), interface energy ( $\Delta\sigma_0$ ), and viscosity ( $\eta$ ) of the melt. These parameters are related by the following pushing/trapping equation:

$$R \propto \frac{\Delta\sigma_0}{\eta r^*}$$

According to the pushing/trapping theory, Y-211 particles of sizes smaller than  $r^*$  will be pushed by the growth front of the Y-123 single grain. In other words, Y-211 particles of size larger than  $r^*$  will be trapped within the growing Y-123 single grain matrix.  $r^*$  is also inversely proportional to the growth rate, which is influenced critically by the under-cooling and the initial Y-211 composition. The values of  $R$  measured for the 40-Y-211, 30-Y-211, and 20-Y-211 samples grown at 998 and 990 °C are listed in Table 3.

Table 3. Growth Rate of 40-Y-211, 30-Y-211, and 20-Y-211 Samples Grown at 998 and 990 °C for Both Growth Directions

	$T_g = 998$ °C		$T_g = 990$ °C	
	$R_{a/b}$ (mm/h)	$R_c$ (mm/h)	$R_{a/b}$ (mm/h)	$R_c$ (mm/h)
40-Y-211	$0.15 \pm 5\%$	$0.19 \pm 4\%$	$0.67 \pm 4\%$	$0.77 \pm 3\%$
30-Y-211	$0.13 \pm 5\%$	$0.20 \pm 4\%$	$0.59 \pm 4\%$	$0.70 \pm 3\%$
20-Y-211	$0.16 \pm 5\%$	$0.14 \pm 5\%$	$0.54 \pm 4\%$	$0.59 \pm 4\%$

It can be seen from Table 3 that the values of  $R$  of all three types of samples grown at 990 °C are higher than those at 998 °C. According to the pushing/trapping theory,  $r^*$  is smaller at 990 °C than at 998 °C, so more Y-211 inclusions will be trapped by the Y-123 single grain grown at 990 °C than at 998 °C. This explains the phenomenon that more Y-211 inclusions are trapped generally when samples are grown under conditions of larger under-cooling temperature.

It is clear from Table 3 that the value of  $R$  in either growth direction increases for the samples processed isothermally at 990 °C, in ascending order, for samples 20-Y-211, 30-Y-211,

and 40-Y-211. Accordingly,  $r^*$  decreases as the initial Y-211 content increases, from which it may be concluded that more Y-211 inclusions are trapped as the initial Y-211 content increases for samples grown at 990 °C.

It can be seen from Table 3 that the value of  $R$  for each sample grown at 998 °C lies within a relatively small range between 0.1 and 0.2 mm/h and that the data exhibits no clear differences. Since the under-cooling temperature is very small, the driving force for the peritectic solidification of the Y-211 and the liquid phases is very small. This leaves sufficient time for the diffusion of  $\text{Y}^{3+}$  atoms and, therefore, a complete peritectic solidification reaction in the vicinity of the seed. The consumption of Y-211 inclusions in the region beneath the seed at smaller under-cooling temperatures tends to be complete, which results in the formation of the low-Y-211 regions in the vicinity of the seed. Therefore, the influence of the initial Y-211 content on the Y-211 inclusions distribution at the low-Y-211 regions formed at the lower under-cooling temperature is not clear.

As the Y-123 single grain grows away from the seed at 998 °C, the volume of the growing Y-123 single grain is increased compared to the volume of the Y-123 phase growing around the seed. Therefore, the need for the supply of  $\text{Y}^{3+}$  is increased as the Y-123 single grain grows away from the seed. In this case, the limiting factor for the growth rate changes gradually from lower under-cooling to the diffusion rate of  $\text{Y}^{3+}$  from the Y-211 inclusions. A higher initial Y-211 content contributes directly to a higher  $\text{Y}^{3+}$  diffusion rate, which, theoretically, would contribute to an increase in the growth rate with the increase of Y-211 contents as the Y-123 single grain grows away from the seed. Moreover, the amount of Y-211 inclusions added in the sample is more than the amount needed for the peritectic reaction; unreacted Y-211 inclusions would remain in the matrix and follow the pushing/trapping theory. According to the analysis above, an increased number of Y-211 contributes to an increased growth rate, which results in a reduced  $r^*$  and therefore an increased number of Y-211 inclusions trapped in the Y-123 single grain as the sample grows away from the seed at 998 °C. This explains the phenomenon that at 998 °C, a low-Y-211 containing region forms beneath the seed area, which is independent of the initial Y-211 contents. The Y-211 inclusion content increases for increasing initial Y-211 content for distances from the seed greater than that of the low-Y-211 region.

The difference in Y-211 inclusion content in the low-Y-211 region fluctuates for the 40-Y-211, 30-Y-211, and 20-Y-211 samples. The P-graded YBCO sample, which consists of only pure Y-211 powder below the seed region, still exhibits a low concentration of Y-211 inclusions close to the position of the seed, which confirms that it is difficult to increase the number of Y-211 particles in the vicinity of the seed by increasing the Y-211 content alone in the initial precursor powder. The N-graded YBCO sample, on the other hand, consisted of 40 wt % Nexans Y-211 powder below the seed region, which corresponds to a higher local concentration and larger Y-211 particle size than other parts of the sample. According to the pushing/trapping theory, Y-211 particles of sizes larger than  $r^*$  will be trapped by the growth front of the Y-123 single grain. Even though the particle size of the Nexans Y-211 powders is relatively large, a low-Y-211 region still exists in the N-graded sample. As we discussed above, this is because when the sample grows from the seed, the under-cooling is relatively small, which tends to completely consume the Y-211 phase in the

vicinity of the seed. Therefore, it can be concluded that a region of low-Y-211 concentration exists below the seed position in YBCO single grains fabricated by TSMG. It is difficult to engineer effective flux pinning centers in the vicinity of the seed in a pure Y-123/Y-211 system given that these are provided largely by the Y-211/Y-123 interface. To introduce more pinning centers into the seed region, it is necessary to introduce inert dopants to the sample microstructure that do not take part in the peritectic reaction. Further studies, therefore, will be performed to attempt to introduce unreacted, second phase pinning centers in the region of the seed, which has significant potential to improve further the superconducting properties of bulk, melt-processed YBCO superconductors for practical applications.

#### 4. CONCLUSION

YBCO samples containing different weight amounts (20, 30, and 40 wt %) of Y-211 were grown in batches by top seeded melt growth using different, isothermal temperature profiles. The peritectic solidification temperature is reduced when the initial Y-211 content is increased in the samples. The self-nucleation temperature and superior temperature growth range were determined for all of the compositions investigated in this study. The growth rate of the Y-123 single grain increases as both the initial Y-211 content increases and as the under-cooling temperature increases. The isothermal growth process has enabled the optimum temperature profile for the growth of YBCO single grains to be determined, which increases the success rate of the TSMG growth of bulk YBCO superconductors and reduces wastage.

The amount of trapped Y-211 inclusions along both the  $a/b$  and  $c$  crystallographic growth directions is increased at larger under-cooling temperature with increased initial Y-211 content. A region of low Y-211 concentration forms in the vicinity of the seed for all three compositions at lower under-cooling temperature. The difference in number of Y-211 inclusions in the low-Y-211 region fluctuates between the 40-Y-211, 30-Y-211, and 20-Y-211 samples. The Y-211 inclusions content increase for the increasing initial Y-211 content as distances from the seed become greater than the low-Y-211 region at lower under-cooling temperature. The low-Y-211 region also exists below the seed position in bulk YBCO single grains, regardless of both the concentration of Y-211 in the precursor powder or the particle size of the Y-211 phase inclusions at the center of the sample. The observed distribution of Y-211 has been explained successfully by a combination of pushing/trapping and Y-diffusion theories. Microstructural analysis of the Y-211 distribution has been used to explain the relation between Y-211 distribution and the measured growth rate. Finally, this analysis has been used to understand the reason for the presence of the low-Y-211 region in bulk YBCO single grains fabricated by TSMG, which, in turn, has indicated the possibility of introducing inert, second phase pinning centers in the vicinity of the seed to grow single grain YBCO samples with improved superconducting properties, which will be the subject of a future study.

#### ■ AUTHOR INFORMATION

##### Corresponding Author

\*E-mail: wz253@cam.ac.uk. Phone: +44 1223 32831.

##### Notes

The authors declare no competing financial interest.

## ■ ACKNOWLEDGMENTS

This work was supported by the Engineering and Physical Sciences Research Council [grant number EP/K02910X/1]. W.Z. acknowledges the financial support from the China Scholarship Council and the Cambridge Commonwealth, European and International Trust.

## ■ REFERENCES

- (1) Campbell, A. M.; Cardwell, D. A. *Cryogenics* **1997**, *37*, 567–575.
- (2) Miyagawa, Y.; Kameno, H.; Takahata, R.; Ueyama, H. *IEEE Trans. Appl. Supercond.* **1999**, *9*, 996–999.
- (3) Hull, J. R. *Supercond. Sci. Technol.* **2000**, *13*, R1–R15.
- (4) Tomita, M.; Murakami, M. *Nature* **2003**, *421* (6922), 517–520.
- (5) Cardwell, D. A. *Mater. Sci. Eng.* **1998**, *B53*, 1–10.
- (6) Morita, M.; Takebayashi, S.; Tanaka, M.; Kimura, K.; Miyamoto, K.; Sawano, K. *Adv. Supercond.* **1991**, *3*, 733–736.
- (7) Salama, K.; Selvamanickam, V.; Gao, L.; Sun, K. *Appl. Phys. Lett.* **1989**, *54* (23), 2352–2354.
- (8) Murakami, M. *Appl. Supercond.* **1993**, *1*, 1157–1173.
- (9) Lo, W.; Cardwell, D. A.; Dung, S. L.; Barter, R. G. *J. Mater. Sci.* **1995**, *30*, 3995–4002.
- (10) Chow, J. C. L.; Lo, W.; Dewhurst, C. D.; Leung, H. T.; Cardwell, D. A.; Shi, Y. H. *Supercond. Sci. Technol.* **1997**, *10*, 435–443.
- (11) Murakami, M. *Mod. Phys. Lett. B* **1990**, *04*, 163.
- (12) Murakami, M. *Supercond. Sci. Technol.* **1992**, *5*, 185–203.
- (13) Goyal, A.; Olivier, W. C.; Funkenbush, P. D.; Kroeger, D. M.; Burns, S. J. *Physica C* **1991**, *183*, 221–233.
- (14) Mathieu, J. P.; Cano, I. G.; Koutzarova, T.; Rulmont, A.; Vanderbemden, Ph.; Dew-Hughes, D.; Ausloos, M.; Cloots, R. *Supercond. Sci. Technol.* **2004**, *17*, 169–174.
- (15) Cloots, R.; Koutzarova, T.; Mathieu, J.-P.; Ausloos, M. *Supercond. Sci. Technol.* **2005**, *18*, R9–23.
- (16) Desgardin, G.; Monot, I.; Raveau, B. *Supercond. Sci. Technol.* **1999**, *12*, R115–R133.
- (17) Izumi, T.; Nakamura, Y.; Shiohara, Y. *J. Mater. Res.* **1992**, *7*, 1621–1628.
- (18) Murakami, M.; Yamaguchi, K.; Fujimoto, H.; Nakamura, N.; Taguchi, T.; Koshizuka, N.; Tanaka, S. *Cryogenics* **1992**, *32*, 930–935.
- (19) Lee, D. F.; Selvamanickam, V.; Salama, I. *Physica C* **1992**, *202*, 83–96.
- (20) Diko, P. *Supercond. Sci. Technol.* **2000**, *13*, 1202–1213.
- (21) Morita, M.; Tanaka, S.; Takebayashi, S.; Kimura, K.; Miyamoto, K.; Sawano, K. *Jpn. J. Appl. Phys.* **1991**, *30*, L813–L815.
- (22) Pinol, S.; Sandiumenge, F.; Martinez, B.; Gomis, V.; Fontcuberta, J.; Obradors, X. *Appl. Phys. Lett.* **1994**, *65*, 1448–1450.
- (23) Chow, J. C. L.; Lo, W.; Leung, H.-T.; Dewhurst, C. D.; Cardwell, D. A. *Mater. Sci. Eng.* **1998**, *B53*, 79–85.
- (24) Endo, A.; Chauhan, H. S.; Egi, T.; Shiohara, Y. *J. Mater. Res.* **1996**, *11*, 795–803.
- (25) Endo, A.; Chauhan, H. S.; Shiohara, Y. *Physica C* **1996**, *273*, 107–119.
- (26) Zhai, W.; Shi, Y. H.; Durrell, J. H.; Dennis, A. R.; Rutter, N. A.; Troughton, S. C.; Speller, S. C.; Cardwell, D. A. *Supercond. Sci. Technol.* **2013**, *26*, 125021.
- (27) Uhlman, D. R.; Chalmer, B.; Jackson, K. A. *J. Appl. Phys.* **1964**, *35*, 2986.
- (28) Xu, K. X.; Wu, X. D.; Qiu, J. H. *Supercond. Sci. Technol.* **2007**, *20*, 969–973.
- (29) Wu, X. D.; Xu, K. X.; Qiu, J. H.; Pan, P. J.; Zhou, K. R. *Physica C* **2008**, *468*, 435–441.
- (30) Shi, Y.; Babu, N. H.; Iida, K.; Cardwell, D. A. *IEEE Trans. Appl. Supercond.* **2007**, *2*, 2984–2987.
- (31) Nakamura, Y.; Endo, A.; Shiohara, Y. *J. Mater. Res.* **1996**, *11* (5), 1094–1100.
- (32) Endo, A.; Chauhan, H. S.; Nakamura, Y.; Shiohara, Y. *J. Mater. Res.* **1996**, *11* (5), 1114–1119.

## ■ NOTE ADDED AFTER ASAP PUBLICATION

This paper was published ASAP on October 29, 2014, with an error to Figure 6 and text referring to Figure 6 content. The corrected version was reposted with the issue on December 3, 2014.